Isomer-delayed γ-ray spectroscopy of $A = 159$–164 midshell nuclei and the variation of K-forbidden $E1$ transition hindrance factors

Z. Patel,[1,2] P. M. Walker,[1] Zs. Podolyák,[1] P. H. Regan,[1,3] T. A. Berry,[1] P.-A. Söderström,[2] H. Watanabe,[2,4,5] E. Ideguchi,[6,7] G. S. Simpson,[8] S. Nishimura,[2] Q. Wu,[9] F. R. Xu,[9] F. Browne,[2,10] P. Doornenbal,[2] G. Lorusso,[2,3] S. Rice,[1,2] L. Sinclair,[2,11] T. Sumikama,[12] J. Wu,[2,9] Z. Y. Xu,[13] N. Aoi,[6,7] H. Baba,[2] F. L. Bello Garrote,[14] G. Benzoni,[15] R. Daido,[7] Zs. Dombrádi,[16] Y. Fang,[7] N. Fukuda,[2] G. Gey,[17] S. Go,[18] A. Gottardo,[19] N. Inabe,[2] T. Isobe,[2] D. Kameda,[2] K. Kobayashi,[20] M. Kobayashi,[18] T. Komatsubara,[2] I. Kojouharov,[21] T. Kubo,[2] N. Kurz,[21] I. Kuti,[16] Z. Li,[22] M. Matsushita,[18] S. Michimasa,[18] C.-B. Moon,[23] H. Nishibata,[7] I. Nishizuka,[12] A. Odahara,[7] E. Şahin,[14] H. Sakurai,[2,13] H. Schaffner,[21] H. Suzuki,[2] H. Takeda,[2] M. Tanaka,[7] J. Taprogge,[24,25] Zs. Vajta,[16] A. Yagi,[7] and R. Yokoyama[18]

[1]*Department of Physics, University of Surrey, Guildford, GU2 7XH, United Kingdom*
[2]*RIKEN Nishina Center, 2-1 Hirosawa, Wako-shi, Saitama 351-0198, Japan*
[3]*National Physical Laboratory, Teddington, Middlesex, TW11 0LW, United Kingdom*
[4]*International Research Center for Nuclei and Particles in the Cosmos, Beihang University, Beijing 100191, China*
[5]*School of Physics and Nuclear Energy Engineering, Beihang University, Beijing 100191, China*
[6]*Research Center for Nuclear Physics (RCNP), Osaka University, Ibaraki, Osaka 567-0047, Japan*
[7]*Department of Physics, Osaka University, Machikaneyama-machi 1-1, Osaka 560-0043 Toyonaka, Japan*
[8]*LPSC, Université Grenoble Alpes, CNRS/IN2P3, Institut National Polytechnique de Grenoble, F-38026 Grenoble Cedex, France*
[9]*School of Physics and State Key Laboratory of Nuclear Physics and Technology, Peking University, Beijing 100871, China*
[10]*School of Computing, Engineering and Mathematics, University of Brighton, Brighton, BN2 4GJ, United Kingdom*
[11]*Department of Physics, University of York, Heslington, York, YO10 5DD, United Kingdom*
[12]*Department of Physics, Tohoku University, Aoba, Sendai, Miyagi 980-8578, Japan*
[13]*Department of Physics, University of Tokyo, Hongo, Bunkyo-ku, Tokyo 113-0033, Japan*
[14]*Department of Physics, University of Oslo, Oslo, Norway*
[15]*INFN Sezione di Milano, I-20133 Milano, Italy*
[16]*Institute for Nuclear Research, Hungarian Academy of Sciences, P. O. Box 51, Debrecen, H-4001, Hungary*
[17]*LPSC, Université Joseph Fourier Grenoble 1, CNRS/IN2P3, Institut National Polytechnique de Grenoble, F-38026 Grenoble Cedex, France*
[18]*Center for Nuclear Study (CNS), University of Tokyo, Wako, Saitama 351-0198, Japan*
[19]*Instituto Nazionale di Fisica Nucleare, Laboratori Nazionali di Legnaro, I-35020 Legnaro, Italy*
[20]*Department of Physics, Rikkyo University, 3-34-1 Nishi-Ikebukuro, Toshima-ku, Tokyo 171-8501, Japan*
[21]*GSI Helmholtzzentrum für Schwerionenforschung GmbH, D-64291 Darmstadt, Germany*
[22]*School of Physics, Peking University, Beijing 100871, China*
[23]*Hoseo University, Asan, Chungnam 336-795, Korea*
[24]*Instituto de Estructura de la Materia, CSIC, E-28006 Madrid, Spain*
[25]*Departamento de Física Teórica, Universidad Autónoma de Madrid, E-28049 Madrid, Spain*

(

Excited states have been studied in ^{159}Sm, ^{161}Sm, ^{162}Sm ($Z = 62$), ^{163}Eu ($Z = 63$), and ^{164}Gd ($Z = 64$), populated by isomeric decay following ^{238}U projectile fission at RIBF, RIKEN. The isomer half-lives range from 50 ns to 2.6 μs. In comparison with other published data, revised interpretations are proposed for ^{159}Sm and ^{163}Eu. The first data for excited states in ^{161}Sm are presented, where a 2.6-μs isomer is assigned a three-quasiparticle, $K^\pi = 17/2^-$ structure. The interpretation is supported by multi-quasiparticle Nilsson-BCS calculations, including the blocking of pairing correlations. A consistent set of reduced $E1$ hindrance factors is obtained. Limited evidence is also reported for isomeric decay in ^{163}Sm, ^{164}Eu, and ^{165}Eu.

I. INTRODUCTION

The rare-earth ($Z = 57$–71) neutron-rich nuclides are good candidates for testing nuclear collectivity because of their midshell position between the closed shells of $Z = 50$ and 82, and $N = 82$ and 126. Furthermore, these nuclides may potentially provide a key to understanding r-process nucleosynthesis and the associated rare-earth abundance peak [1]. However, their neutron excess makes experimental access difficult, and recent progress has to a large extent depended on the presence of isomeric states. Isomers in deformed nuclides are most abundant in the $A \sim 180$ region above midshell [2–4], but there have been several recent discoveries in the midshell region and below, i.e., in the neutron-rich, $A = 160$–170 region, exploiting mass-separated isomeric beams, e.g., Refs. [5–10]. In such cases, the existence of high-spin isomers provides a useful tool to probe the excited-state structure of nuclei that are otherwise difficult to populate.

Isomers in deformed nuclides are associated with the K quantum number, which is the projection of the angular

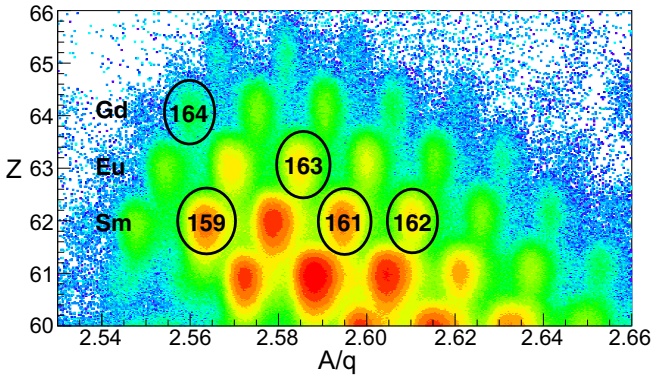

FIG. 1. Atomic number Z vs mass-to-charge ratio A/q, giving particle identification for fully stripped neutron-rich midshell nuclei. Level structures for all circled nuclides are discussed in this work.

momentum of a nucleus on its symmetry axis. A nucleus may become "trapped" in an aligned spin orientation [2] when the transition to a lower energy state with a different K value is forbidden by the selection rule, $\Delta K \leqslant \lambda$, where λ is the multipole order of the transition. In practice, these transitions are able to proceed through symmetry-breaking processes, with hindrance factors that are strongly correlated with the degree of forbiddenness, $\nu = \Delta K - \lambda$ [3].

The present work exploits these K-isomer features to study excited states in several well-deformed, neutron-rich nuclides. Previous related studies [10–12] are discussed and some revised interpretations are proposed.

II. EXPERIMENT

Neutron-rich nuclei were produced at the Radioactive Isotope Beam Factory (RIBF), RIKEN, Japan, by in-flight fission of a 345 A MeV ^{238}U beam with an average beam intensity of 10 particle-nA incident on a ^{9}Be target. The isotopes of interest were separated and identified according to their mass-to-charge ratio (A/q) and atomic number (Z) using the BigRIPS and ZeroDegree spectrometers [13,14]. BigRIPS

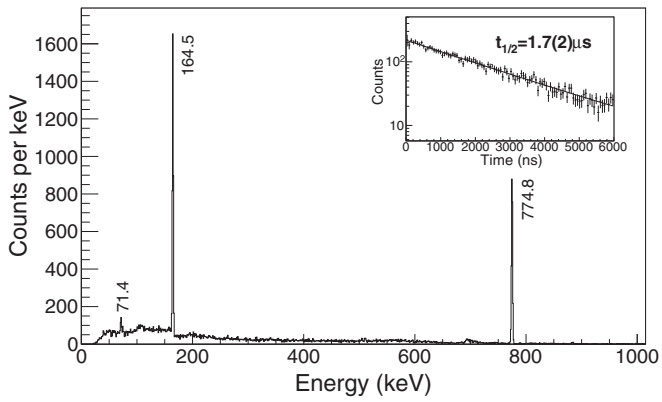

FIG. 2. Energy spectrum of delayed γ rays from ^{162}Sm observed within 3.0 μs following implantation. (Inset) The exponential decay curve from the isomeric decay of ^{162}Sm, obtained from the 165- and 775-keV γ rays, using 60 ns/bin.

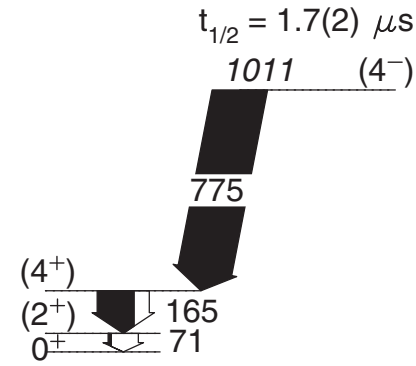

FIG. 3. Level scheme of ^{162}Sm obtained in this work. Internal conversion electron intensity is represented in white, and γ-ray intensity is in black.

is a two-stage achromatic separator based on magnetic rigidity and energy loss, employing the $B\rho - \Delta E - B\rho$ method and, together with the time of flight in the ZeroDegree spectrometer, ion-by-ion identification is achieved by $B\rho - \mathrm{TOF} - \Delta E$ analysis. The flight time of approximately 0.7-μs limits the minimum half-life that can be detected, although this depends also on the yield, and on the electron conversion coefficient, because no electron conversion is possible for fully stripped ions.

Delayed γ rays were detected from the isomeric decay of the ions implanted in a copper passive stopper at the center of EURICA (Euroball-RIKEN Cluster Array), which consisted of 84 HPGe crystals arranged in a 4π configuration at ~22 cm from the implantation point [15–17]. A 100-μs window was used to time correlate ion implantation with γ-ray detection. The absolute efficiency of the array was 16.6% at 100 keV and 7.6% at 1 MeV.

III. RESULTS

A particle identification plot based on Z and A/q is shown in Fig. 1, from which 2D particle gates were set for all nuclides with $62 \leqslant Z \leqslant 64$, and delayed γ-ray spectra were created. The results for ^{160}Sm [7], and ^{164}Sm and ^{166}Gd [6], have been reported earlier. In the present work, we show results for the other nuclides where isomeric states were identified, i.e., ^{159}Sm, ^{161}Sm, ^{162}Sm, ^{163}Eu, and ^{164}Gd, which are circled in Fig. 1. To see each γ-ray energy spectrum clearly, a variable time gate was made in the energy-time matrix to reduce as much as possible the implantation-induced prompt flash, without rejecting useful data. At low energies the useful observation time of the γ rays is from ~0.5 μs, whereas at

TABLE I. Energy levels and transitions in ^{162}Sm from the present work. Total intensities include electron conversion calculated [18] according to the assigned spins and parities.

E_i (keV)	J_i^π	E_γ (keV)	B_{tot}(rel.)	I_{tot}(rel.)	I_γ(rel.)	J_f^π
71.4(4)	(2^+)	71.4(4)	100	56(20)	6(2)	0^+
235.9(5)	(4^+)	164.5(3)	100	95(5)	68(3)	(2^+)
1010.7(6)	(4^-)	774.8(3)	100	100(5)	100(5)	(4^+)

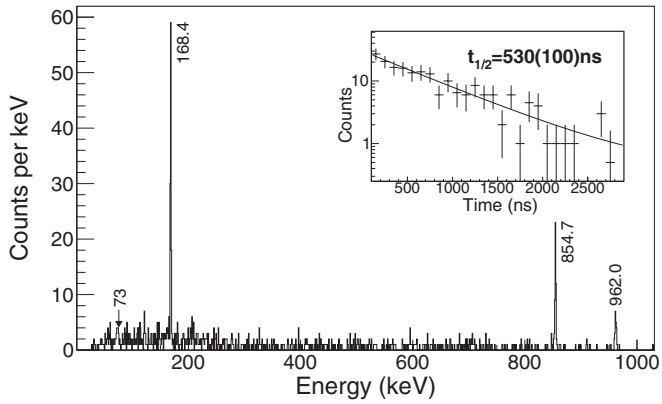

FIG. 4. Spectrum of γ rays from ^{164}Gd, emitted within 1.4 μs after an ion's arrival. (Inset) The exponential decay curve from the isomeric decay of ^{164}Gd, using 30-ns binning.

high energies (i.e., >200 keV) the prompt flash is narrower, and so the gate can be made within 100 ns of ion implantation. The particle gate together with the variable time gate were used to produce γ-ray energy spectra. When determining the γ-ray intensities and half-lives, a fixed time range was used for a given nuclide. When fitting each half-life, a single exponential decay was assumed, on top of a constant background. The construction of level schemes made use of γ-ray coincidence relationships (within a 400-ns time window), where available.

Spin assignments are tentative on account of the lack of angular correlations or directly measured electron conversion coefficients. Nevertheless, where an isomer populates a rotational band, a regular rotational structure is expected, with spacings that match the systematics for the appropriate quasiparticle (qp) configuration. The isomer itself is then assumed to decay mainly by dipole transitions. Furthermore, if a pathway is available for quadrupole decay, but no transition is observed, then a parity change is inferred, i.e., $E2$ transitions should be seen, but not $M2$ transitions. This latter inference is relatively weak, but forms a useful starting point for further discussion of possible isomer configurations, in comparison with theoretical calculations.

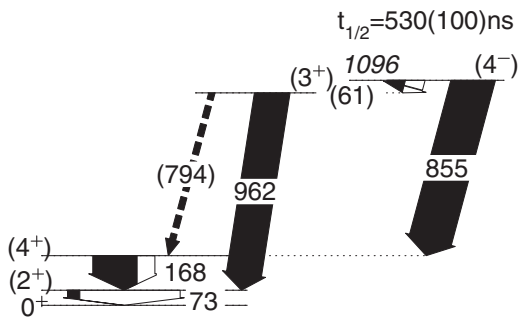

FIG. 5. Level scheme of ^{164}Gd obtained in this work. Internal conversion electron intensity is represented in white, and γ-ray intensity is in black.

TABLE II. Energy levels and transitions in ^{164}Gd from the present work. Total intensities include electron conversion calculated [18] according to the assigned spins and parities. Transitions marked with * are unobserved but inferred from coincidence relationships. Intensities marked † have not been directly measured but are obtained from the intensity balance of incoming and outgoing transitions.

E_i (keV)	J_i^π	E_γ (keV)	B_{tot}(rel.)	I_{tot}(rel.)	I_γ(rel.)	J_f^π
73(1)	(2^+)	73(1)	100	180(93)	27(14)	0^+
241.1(11)	(4^+)	168.4(4)	100	100(28)	100(28)	(2^+)
1034.9(11)	(3^+)	961.9(4)	100	56(12)	79(17)	(2^+)
1096.1(12)	(4^-)	61(1)*	45(14)†	56(12)†	16(6)†	(3^+)
		854.7(5)	55(17)	69(24)	97(34)	(4^+)

A. ^{162}Sm and ^{164}Gd results

The even-even nuclides ^{162}Sm and ^{164}Gd present relatively simple γ-ray spectra, and they usefully confirm the Z and A/q calibrations of Fig. 1. Although their isomers have been identified by Yokoyama *et al.* [10] with a pre-EURICA setup at RIBF, the new data are independent and are supported by γ-ray coincidence relationships. Also, the ^{162}Sm isomer was identified in the β decay of ^{162}Pm [12].

Three γ-ray transitions are visible in the energy spectrum of ^{162}Sm (Fig. 2). However, one of them is from the low energy $2^+ \rightarrow 0^+$ transition, which is normally difficult to observe in this type of experiment because of the high electron conversion coefficient and the large Compton background from the other detected γ rays. The measured half-life of the isomeric state is 1.7(2) μs, as shown in Fig. 2 (inset).

The level scheme, constructed with the aid of γ-γ coincidences, is shown in Fig. 3 and the intensities are given in Table I. The intensity through the 2^+ level in the rotational band does not balance. This is likely because of the large uncertainty in the efficiency of the germanium detectors at low energies ($E < 80$ keV) and the large background radiation at this energy. Spin and parity assignments are tentative in the absence of angular correlations. Nilsson-BCS calculations support the (4^-) spin-parity assignment for the isomeric state (Sec. IV A). The data are in agreement with Yokoyama *et al.* [10], who reported a half-life of 1.78(7) μs.

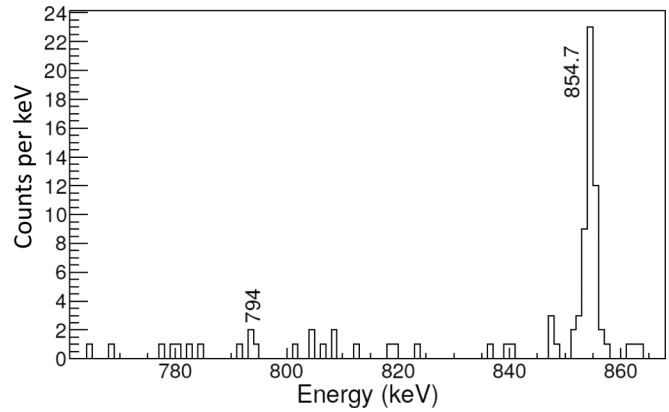

FIG. 6. Enlarged view of the possible 794-keV transition in ^{164}Gd.

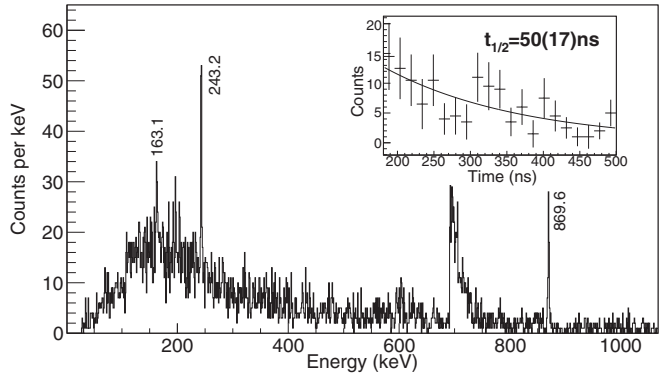

FIG. 7. Energy spectrum of delayed γ rays from ^{159}Sm emitted within 800 ns of an ion's arrival. (Inset) The exponential decay curve from the decay of the isomeric state in ^{159}Sm, obtained from all labeled γ rays, with 14-ns binning.

An energy spectrum of ^{164}Gd γ rays is shown in Fig. 4 from the present work. The ground-state band had been identified up to spin (14^+) following spontaneous fission by Jones *et al.* [19], and Osa *et al.* [20] reported γ rays from β decay, including a 168.8-keV transition. The present work confirms the identification of the 168-keV γ ray as originating from ^{164}Gd.

The half-life of the ^{164}Gd isomer was measured to be 530(100) ns from the weighted averages of the 168- and 855-keV γ rays. The level scheme was constructed with the aid of γ-γ coincidences. This is shown in Fig. 5, with intensities in Table II. The isomeric state is assigned a $K^\pi = (4^-)$ spin parity and is supported by Nilsson-BCS calculations presented in Sec. IV A. The (3^+) state is likely part of the γ band, with $K^\pi = 2^+$. The 61-keV transition is inferred from coincidence relationships. These features of the level scheme are in agreement with the data of Yokoyama *et al.* [10], who obtained a half-life of 580(23) ns, and clearly observed the 61-keV transition. In addition, we now have tentative evidence for a 794-keV transition between the (3^+) and (4^+) states, as illustrated in Fig. 6. A summary of transition intensities is given in Table II.

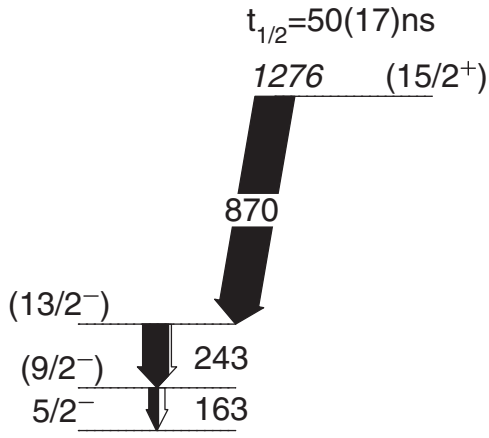

FIG. 8. Partial level scheme of ^{159}Sm in this work. Internal conversion electron intensity is represented in white, and γ-ray intensity is in black.

TABLE III. Energy levels and transitions in ^{159}Sm from the present work. Total intensities include electron conversion calculated [18] according to the assigned spins and parities.

E_i (keV)	J_i^π	E_γ (keV)	B_{tot}(rel.)	I_{tot}(rel.)	I_γ(rel.)	J_f^π
163.1(9)	$(\frac{9}{2}^-)$	163.1(9)	100	36(14)	25(10)	$(\frac{5}{2}^-)$
406(1)	$(\frac{13}{2}^-)$	243.2(7)	100	74(23)	67(21)	$(\frac{9}{2}^-)$
1276(1)	$(\frac{15}{2}^+)$	869.6(8)	100	100(37)	100(31)	$(\frac{13}{2}^-)$

B. ^{159}Sm results

The γ rays associated with the isomeric decay of ^{159}Sm are shown in Fig. 7. This isomer was previously identified by Urban *et al.* [11] from spontaneous-fission studies. Prior to their work, the 163-243-870 keV cascade was reported as belonging to ^{154}Nd [21]. The particle identification of the present work (Fig. 1) definitively confirms the interpretation of Urban *et al.* that this cascade belongs to ^{159}Sm. The partial level scheme found in the present work can be seen in Fig. 8. The transition intensities are summarized in Table III. Urban *et al.* measured the half-life of the isomer as 116(8) ns with higher statistics than in the present work, where the half-life was measured to be 50(17) ns from the weighted average of the three observed γ-ray transitions.

The $\frac{5}{2}^-$ ground state in Fig. 8 was previously assigned the $\nu\frac{5}{2}^-[523]$ configuration by Urban *et al.* The assignment is supported by Nilsson-BCS calculations, presented in Sec. IV B. According to Urban *et al.*, the isomeric state is from the $\nu\frac{11}{2}^-[505]$ intruder orbital. However, in the present work the isomeric state is assigned $K = (\frac{15}{2}^+)$ because of the lack of an observed transition from the isomeric state to either the $(\frac{9}{2}^-)$ state, or the $(\frac{11}{2}^-)$ member (not shown) of the $\nu\frac{5}{2}^-[523]$ band. This issue is further discussed in Sec. IV B.

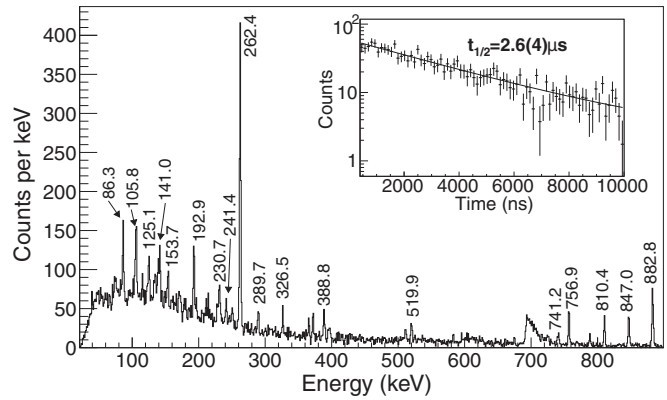

FIG. 9. Energy spectrum of delayed γ rays from ^{161}Sm observed within 3.0 μs following implantation. (Inset) The exponential decay curve from the isomeric decay of ^{161}Sm, obtained from the 262-keV transition, with 120-ns binning.

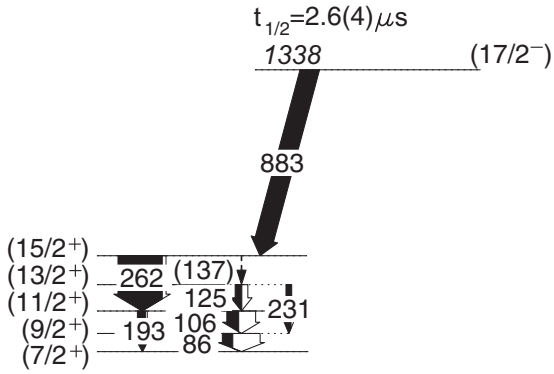

FIG. 10. Partial level scheme of ^{161}Sm from the present work.

C. ^{161}Sm results

The γ rays associated with ^{161}Sm can be seen in Fig. 9. Prior to this work only its β-decay half-life of 4.8(4) s was measured by Ichikawa *et al.* [22], and no excited-state structure had been identified. Unlike the isomer in odd-even ^{159}Sm, the half-life of the isomer in ^{161}Sm is relatively long, 2.6(4) μs [compared to 50(17) ns], as shown in Fig. 9. A partial level scheme is illustrated in Fig. 10, and an example gated γ-ray coincidence spectrum is shown in Fig. 11. Several of the weaker transitions could not be placed in the scheme. Nevertheless, using also $N = 99$ energy-level systematics [23] (including the rotational band spacings), the population of a rotational band based on the $\frac{7}{2}^+[633]$ neutron looks clear, leading to a probable $K^\pi = (\frac{17}{2}^-)$ spin assignment for the isomer. A complication is that the intensity flow implies that the 262-keV transition is a doublet, but this could not be resolved. Transition assignments and intensities are given in Table IV, and comparison with Nilsson-BCS calculations is made in Sec. IV C.

D. ^{163}Eu results

Prior to this work, the β decay of ^{163}Eu was identified by Osa *et al.* [20] with a half-life of 7.7(4) s. Very recently, Yokoyama *et al.* [10] presented a level scheme based on isomer depopulation, which is very similar to what we now propose. The isomer-delayed γ-ray spectrum observed in the present work is shown in Fig. 12.

The half-life of the isomeric state in ^{163}Eu was measured to be 990(40) ns, from the weighted averages of the decay curves of the 214- and 675-keV γ rays. This compares with 869(29) ns obtained by Yokoyama *et al.* [10]. The level scheme from the present work is given in Fig. 13, and a summary of the transition intensities is found in Table V. The spins and parities of the rotational levels were assigned to be consistent with a band based on the $\frac{5}{2}^+[413]$ neutron, from $Z = 63$ systematics, and Nilsson-BCS calculations, as discussed in Sec. IV D. The main decay path is through the 675-214-75 keV transitions from the isomeric state, with the tentative $(\frac{13}{2}^-)$ isomer spin assignment coming from assumed dipole character for the

TABLE IV. Energy levels and transitions in ^{161}Sm from the present work. Total intensities include electron conversion calculated [18] according to the assigned spins and parities.

E_i (keV)	J_i^π	E_γ (keV)	B_{tot}(rel.)	I_{tot}(rel.)	I_γ(rel.)	J_f^π
86.3(4)	$(\frac{9}{2}^+)$	86.3(4)	100	79(16)	24(5)	$(\frac{7}{2}^+)$
192.9(4)	$(\frac{11}{2}^+)$	105.8(4)	74(15)	61(11)	27(5)	$(\frac{9}{2}^+)$
		192.9(4)	26(5)	21(3)	18(3)	$(\frac{7}{2}^+)$
317.6(5)	$(\frac{13}{2}^+)$	125.1(5)	68(26)	26(10)	15(6)	$(\frac{11}{2}^+)$
		230.7(6)	32(11)	12(4)	12(4)	$(\frac{9}{2}^+)$
455.3(5)	$(\frac{15}{2}^+)$	137.0(10)	14(6)	16(6)	10(4)	$(\frac{13}{2}^+)$
		262.4(3)	86(4)	100(2)	100(2)	$(\frac{11}{2}^+)$
1338.1(6)	$(\frac{17}{2}^-)$	882.8(4)	≈70	40(6)	43(6)	$(\frac{15}{2}^+)$
Unplaced		141.0(5)			19(5)	
		326.5(4)			8(2)	
		519.9(5)			8(2)	
		741.2(6)			19(4)	
		756.9(4)			9(3)	
		847.0(4)			18(4)	

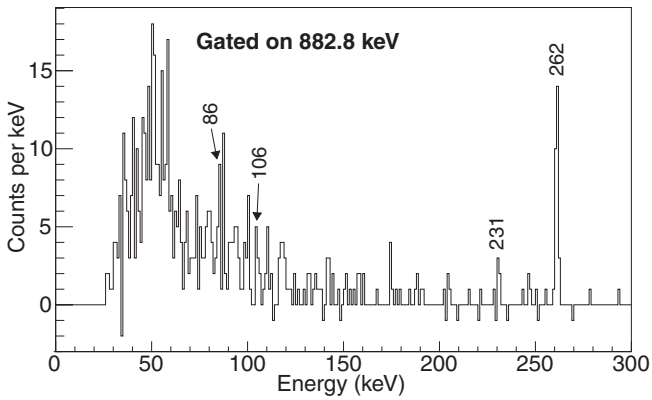

FIG. 11. Background-subtracted energy spectrum for ^{161}Sm, gated on the 883-keV transition, showing, among others, the 262-keV transition.

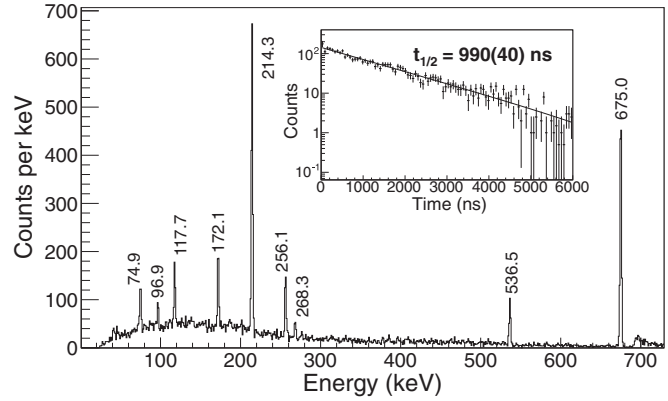

FIG. 12. Spectrum of γ rays from ^{163}Eu, emitted within 2.5 μs after an ion's arrival. (Inset) The exponential decay curve from the isomeric decay of ^{163}Eu with 60 ns/bin.

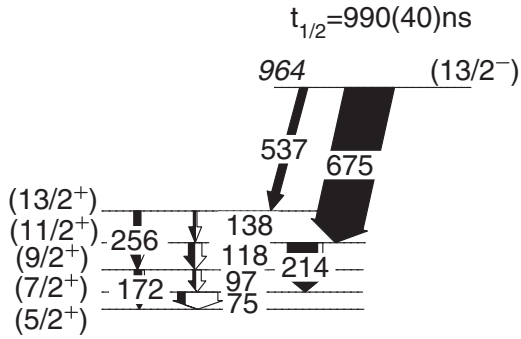

FIG. 13. Level scheme of ^{163}Eu obtained in this work. The 138-keV transition can only be seen in coincidence spectra. Internal conversion electron intensity is represented in white; γ-ray intensity is in black.

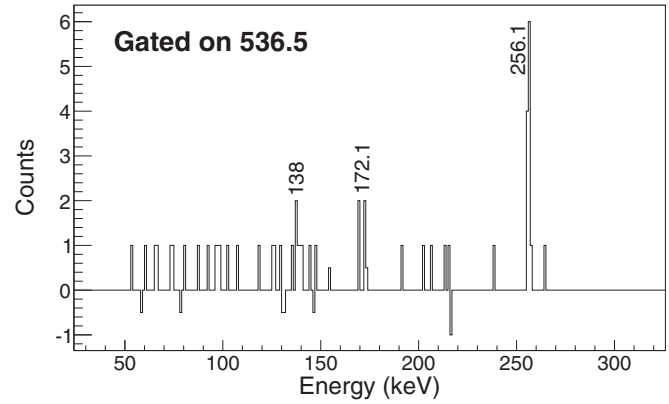

FIG. 14. Background-subtracted energy spectrum for ^{163}Eu, gated on the 537-keV transition, showing, among others, the 138-keV transition.

537- and 675-keV transitions, and the absence of an observed transition to the $\frac{9}{2}^+$ band member.

The 268-keV transition was not placed, while the placement of the 138-keV transition is based on the observation of coincidences in the 537-keV gate, as shown in Fig. 14. The resulting level scheme (Fig. 13) is very similar to that of Yokoyama *et al.* [10], although with the ordering of the 537- and 256-keV transitions reversed. This is determined both by the regularity of the $K^\pi = \frac{5}{2}^+$ band spacing, and by the coincidence relationships.

E. Other isomers

Relatively low-intensity isomeric γ-ray decay was observed in ^{163}Sm (at 197, 221, and 382 keV), ^{164}Eu (at 53.7, 89.5, 120.4, and 214 keV), and ^{165}Eu (at 124.2, 156, and 244 keV) [24] but level schemes could not be constructed. Energy spectra are shown in Figs. 15–17. Their half-lives are in the μs domain.

TABLE V. Energy levels and transitions in ^{163}Eu from the present work. Total intensities include electron conversion calculated [18] according to the assigned spins and parities. The transition marked with * is only visible in coincidence spectra.

E_i (keV)	J_i^π	E_γ (keV)	B_{tot}(rel.)	I_{tot}(rel.)	I_γ(rel.)	J_f^π
74.9(4)	$(\frac{7}{2}^+)$	74.9(4)	100	82(16)	16(3)	$(\frac{5}{2}^+)$
172.1(4)	$(\frac{9}{2}^+)$	96.9(5)	44(20)	17(7)	6(2)	$(\frac{7}{2}^+)$
		172.1(4)	56(13)	21(3)	16(2)	$(\frac{5}{2}^+)$
289.8(7)	$(\frac{11}{2}^+)$	117.7(4)	27(4)	27(4)	13(2)	$(\frac{9}{2}^+)$
		214.3(3)	73(6)	73(5)	63(4)	$(\frac{7}{2}^+)$
428.2(7)	$(\frac{13}{2}^+)$	138(1)*	11(6)	2(1)	1.2(6)	$(\frac{11}{2}^+)$
		256.1(4)	89(12)	15(2)	14(2)	$(\frac{9}{2}^+)$
964.2(6)	$(\frac{13}{2}^-)$	536.5(4)	14(2)	17(2)	17(2)	$(\frac{13}{2}^+)$
		675.0(3)	86(6)	100(7)	100(7)	$(\frac{11}{2}^+)$

IV. MULTI-QUASIPARTICLE CALCULATIONS

Nilsson-BCS calculations were performed for comparison with the level schemes, using a code developed by Jain *et al.* [25]. The pairing strengths were fixed as $G_\pi = 21.00$ A MeV and $G_\nu = 20.00$ A MeV for all nuclides, in accordance with Jain *et al.* [25]. The average uncertainty in the energies is estimated to be ~200 keV. However, the uncertainty can be as much as 400 keV [26]. Residual spin-spin interactions are approximately accounted for by adding 200 keV to the energies of unfavored configurations. Like-particle couplings (protons or neutrons) with the same spin orientation are unfavored, as are unlike particles with opposite spin orientations [27].

A. ^{162}Sm and ^{164}Gd Nilsson-BCS calculations

To support the spin-parity assignments in the ^{162}Sm and ^{164}Gd level schemes, Nilsson-BCS calculations [25] have been performed. The Nilsson energies were calculated with deformation parameters $\epsilon_2 = 0.275$ and $\epsilon_4 = -0.007$ (^{162}Sm), and $\epsilon_2 = 0.275$ and $\epsilon_4 = 0.007$ (^{164}Gd) taken from Möller *et al.* [28]. The results can be seen in Tables VI and VII.

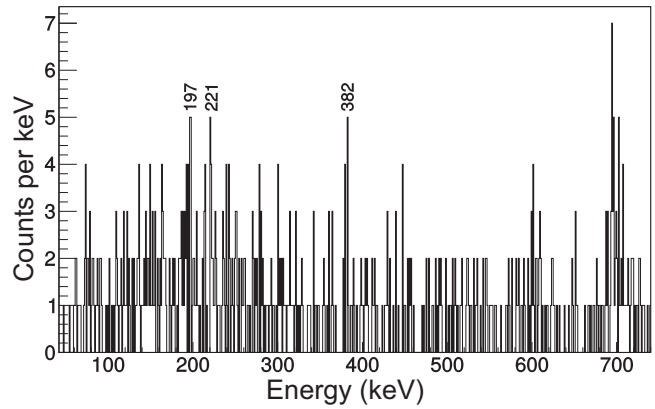

FIG. 15. Energy spectrum of ^{163}Sm, observed up to 0.5 μs following implantation, with candidate delayed γ rays labeled. (The peak at ~695 keV is contamination from neutron scattering.)

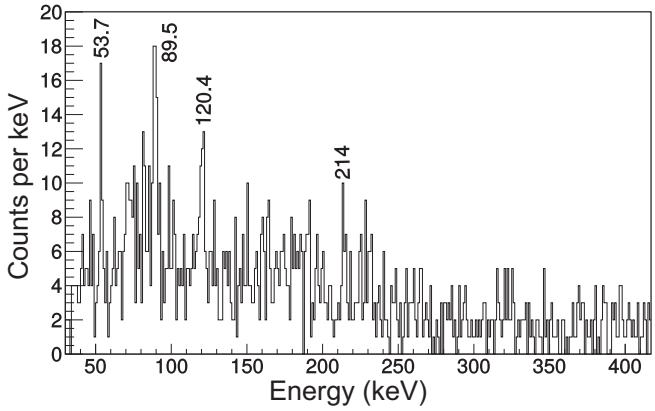

FIG. 16. Energy spectrum of ^{164}Eu, observed up to 2 μs following implantation, with candidate delayed γ rays labeled.

The lowest-energy 2-qp state calculated for ^{162}Sm has a $K^\pi = 5^-$, two-proton configuration, $\pi\frac{5}{2}^-[532] \otimes \pi\frac{5}{2}^+[413]$. However, it is likely that the 6^+ state in the ground-state band would be populated significantly if the isomeric state has a 5^- spin parity. Because population of the 6^+ state is not observed, the assignment of 5^- spin parity to the isomeric state is rejected. The next-lowest energy state calculated has a two-neutron $\nu\frac{1}{2}^-[521] \otimes \nu\frac{7}{2}^+[633]$ configuration, which gives a spin parity of 4^-, in agreement with the experimental assignment in Fig. 3. The measured and calculated energies are in good agreement. For ^{164}Gd, the calculations (Table VII) are in agreement with the same 4^- assignment for the isomeric state (Fig. 5) and the same two-neutron configuration. This is not surprising, as the two nuclides are isotones, with $N = 100$. The measured and calculated energies are again in good agreement. The resulting interpretations are in accord with those reported by Yokoyama *et al.* [10].

B. ^{159}Sm Nilsson-BCS calculations

Nilsson-BCS calculations have been performed to further understand the level scheme of ^{159}Sm. The deformation parameters were taken from Möller *et al.* [28]: $\epsilon_2 = 0.267$ and $\epsilon_4 = -0.033$. The results can be seen in Table VIII. The 1-qp $\frac{3}{2}^-$, $\frac{5}{2}^+$, and $\frac{7}{2}^+$ states predicted for ^{159}Sm are significantly higher in energy than the 1-qp $\frac{5}{2}^-$ state, consistent with a $\nu\frac{5}{2}^-[523]$ ground-state configuration assignment. In

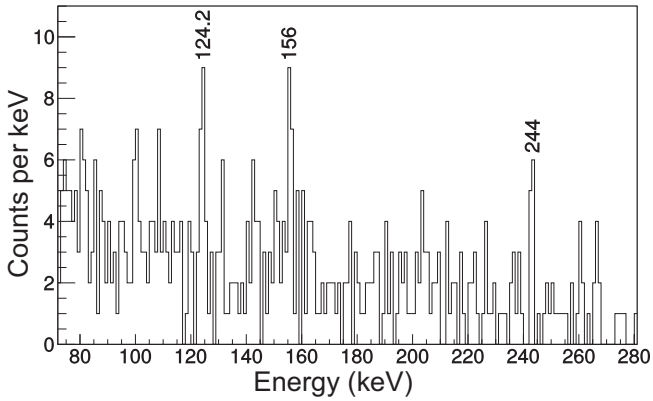

FIG. 17. Energy spectrum of ^{165}Eu, observed up to 2 μs following implantation, with candidate delayed γ rays labeled.

TABLE VI. Low-lying qp states in ^{162}Sm predicted by Nilsson-BCS calculations. The calculations have only been performed for the lowest energy (near yrast) states. An energy of 200 keV was added to those marked with * as they have energetically unfavored configurations according to the residual spin-spin coupling rules.

K^π	Configuration	E_x (MeV)	$E_x^{\rm exp}$ (MeV)
ν 2-qp			
4^-	$\nu\frac{1}{2}^-[521] \otimes \nu\frac{7}{2}^+[633]$	1.043	1.011(1)
6^-	$\nu\frac{7}{2}^+[633] \otimes \nu\frac{5}{2}^-[512]$	1.797*	
6^-	$\nu\frac{7}{2}^+[633] \otimes \nu\frac{5}{2}^-[523]$	1.940	
7^-	$\nu\frac{7}{2}^+[633] \otimes \nu\frac{7}{2}^-[514]$	2.340	
π 2-qp			
5^-	$\pi\frac{5}{2}^-[532] \otimes \pi\frac{5}{2}^+[413]$	1.000	
4^-	$\pi\frac{5}{2}^-[532] \otimes \pi\frac{3}{2}^+[411]$	1.547*	
4-qp			
9^+	$\nu\frac{1}{2}^-[521] \otimes \nu\frac{7}{2}^+[633]$, $\pi\frac{5}{2}^-[532] \otimes \pi\frac{5}{2}^+[413]$	2.043	
8^+	$\nu\frac{7}{2}^+[633] \otimes \nu\frac{1}{2}^-[521]$, $\pi\frac{5}{2}^-[532] \otimes \pi\frac{5}{2}^+[413]$	2.390	
11^+	$\nu\frac{5}{2}^-[523] \otimes \nu\frac{7}{2}^+[633]$, $\pi\frac{5}{2}^-[532] \otimes \pi\frac{5}{2}^+[413]$	2.940	

TABLE VII. Low-lying qp states in ^{164}Gd, as for ^{162}Sm (see Table VI header).

K^π	Configuration	E_x (MeV)	$E_x^{\rm exp}$ (MeV)
ν 2-qp			
4^-	$\nu\frac{1}{2}^-[521] \otimes \nu\frac{7}{2}^+[633]$	1.052	1.096(1)
6^-	$\nu\frac{7}{2}^+[633] \otimes \nu\frac{5}{2}^-[512]$	1.799*	
7^-	$\nu\frac{7}{2}^+[633] \otimes \nu\frac{7}{2}^-[514]$	2.323	
π 2-qp			
4^-	$\pi\frac{3}{2}^+[411] \otimes \pi\frac{5}{2}^-[532]$	1.500*	
4^+	$\pi\frac{3}{2}^+[411] \otimes \pi\frac{5}{2}^+[413]$	1.317	
5^-	$\pi\frac{5}{2}^+[413] \otimes \pi\frac{5}{2}^-[532]$	1.631	
4-qp			
8^-	$\nu\frac{1}{2}^-[521] \otimes \nu\frac{7}{2}^+[633]$, $\pi\frac{3}{2}^+[411] \otimes \pi\frac{5}{2}^+[413]$	2.169	
8^+	$\nu\frac{7}{2}^+[633] \otimes \nu\frac{1}{2}^-[521]$, $\pi\frac{5}{2}^-[532] \otimes \pi\frac{3}{2}^+[411]$	2.552*	
9^+	$\nu\frac{1}{2}^-[521] \otimes \nu\frac{7}{2}^+[633]$, $\pi\frac{5}{2}^-[532] \otimes \pi\frac{5}{2}^+[413]$	2.683	

TABLE VIII. Low-lying qp states in ^{159}Sm, as for ^{162}Sm (see Table VI header).

K^π	Configuration	E_x (MeV)	E_x^{exp} (MeV)
1-qp states			
$\frac{5}{2}^-$	$\nu\frac{5}{2}^-[523]$	0	
$\frac{3}{2}^-$	$\nu\frac{3}{2}^-[521]$	0.490	
$\frac{5}{2}^+$	$\nu\frac{5}{2}^+[642]$	0.518	
$\frac{7}{2}^+$	$\nu\frac{7}{2}^+[633]$	0.589	
$\frac{11}{2}^-$	$\nu\frac{11}{2}^-[505]$	1.255	
3-qp states			
$\frac{15}{2}^+$	$\nu\frac{5}{2}^-[523]\otimes\pi\frac{5}{2}^-[532]\otimes\pi\frac{5}{2}^+[413]$	1.040	1.276(1)
$\frac{13}{2}^+$	$\nu\frac{3}{2}^-[521]\otimes\pi\frac{5}{2}^-[532]\otimes\pi\frac{5}{2}^+[413]$	1.530	
$\frac{15}{2}^-$	$\nu\frac{5}{2}^+[642]\otimes\pi\frac{5}{2}^-[532]\otimes\pi\frac{5}{2}^+[413]$	1.559	
$\frac{13}{2}^+$	$\nu\frac{5}{2}^-[523]\otimes\pi\frac{5}{2}^-[532]\otimes\pi\frac{3}{2}^+[411]$	1.572*	
$\frac{15}{2}^+$	$\nu\frac{5}{2}^-[523]\otimes\nu\frac{3}{2}^-[521]\otimes\nu\frac{7}{2}^+[633]$	1.581	
$\frac{17}{2}^-$	$\nu\frac{7}{2}^+[633]\otimes\pi\frac{5}{2}^-[532]\otimes\pi\frac{5}{2}^+[413]$	1.630	

TABLE IX. Low-lying qp states in ^{161}Sm, as for ^{162}Sm (see Table VI header).

K^π	Configuration	E_x (MeV)	$E_x^{\rm exp}$ (MeV)
1-qp states			
$\frac{7}{2}^+$	$\nu\frac{7}{2}^+[633]$	0	
$\frac{1}{2}^-$	$\nu\frac{1}{2}^-[521]$	0.062	
$\frac{5}{2}^-$	$\nu\frac{5}{2}^-[523]$	0.351	
$\frac{5}{2}^-$	$\nu\frac{5}{2}^-[512]$	0.502	
3-qp states			
$\frac{17}{2}^-$	$\nu\frac{7}{2}+[633]\otimes\pi\frac{5}{2}^-[532]\otimes\pi\frac{5}{2}^+[413]$	1.014	1.338(1)
$\frac{11}{2}^+$	$\nu\frac{1}{2}^-[521]\otimes\pi\frac{5}{2}^-[532]\otimes\pi\frac{5}{2}^+[413]$	1.075	
$\frac{13}{2}^+$	$\nu\frac{5}{2}^-[523]\otimes\nu\frac{1}{2}^-[521]\otimes\nu\frac{7}{2}^+[633]$	1.365	
$\frac{15}{2}^+$	$\nu\frac{5}{2}^-[512]\otimes\pi\frac{5}{2}^-[532]\otimes\pi\frac{5}{2}^+[413]$	1.516	
$\frac{15}{2}^-$	$\nu\frac{7}{2}^+[633]\otimes\pi\frac{5}{2}^-[532]\otimes\pi\frac{3}{2}^+[411]$	1.560*	
$\frac{15}{2}^+$	$\nu\frac{5}{2}^-[523]\otimes\pi\frac{5}{2}^-[532]\otimes\pi\frac{3}{2}^+[411]$	1.564*	
$\frac{17}{2}^+$	$\nu\frac{5}{2}^-[523]\otimes\nu\frac{5}{2}^-[512]\otimes\nu\frac{7}{2}^+[633]$	1.705	
$\frac{19}{2}^+$	$\nu\frac{11}{2}^-[505]\otimes\nu\frac{1}{2}^-[521]\otimes\nu\frac{7}{2}^+[633]$	2.161	

addition, the 3-qp $\frac{15}{2}^+$ state is significantly lower in energy than the other calculated 3-qp states, and supports the assignment of $K^\pi = (\frac{15}{2}^+)$ for the isomeric state in Fig. 8, with a $\nu\frac{5}{2}^-[523]\otimes\pi\frac{5}{2}^-[532]\otimes\pi\frac{5}{2}^+[413]$ configuration. The experimental energy of the isomeric state [1276(1) keV] is within 250 keV of the calculated energy (1040 keV) which is reasonable, given that the error in the calculated values is ~200 keV [25]. Urban *et al.* [11] previously assigned the isomeric state as an $\frac{11}{2}^-$ intruder state. However, because of a lack of transitions from the isomeric state to the $(\frac{13}{2}^-)$ and $(\frac{9}{2}^-)$ levels in the rotational band, and with support from the Nilsson-BCS calculations, a $K^\pi = (\frac{15}{2}^+)$ assignment is preferred.

Urban *et al.* [11] also observed a rotational band built on the isomer, so further comment on that assignment is appropriate. First, the in-band γ-ray branching ratios were not consistent with their model predictions for an $\frac{11}{2}^-[505]$ structure; neither are they consistent with our proposed 3-qp configuration. However, they would be consistent with the $K^\pi = \frac{15}{2}^-$, $\nu\frac{5}{2}^+[642]\otimes\pi\frac{5}{2}^-[532]\otimes\pi\frac{5}{2}^+[413]$ configuration, calculated at higher energy (Table VIII). Indeed, for $K = \frac{15}{2}$, the band has a significant degree of rotational alignment (or, equivalently, a relatively high moment of inertia) which suggests the involvement of an $i_{13/2}$ neutron, supporting the inclusion of the $\frac{5}{2}^+[642]$ neutron component. We suggest, therefore, that there is a missing, possibly low energy, transition from the $K^\pi = \frac{15}{2}^-$ bandhead to the $K^\pi = \frac{15}{2}^+$ isomer. Clearly, this goes beyond the scope of the present work, and indicates the need for additional experimental data.

C. ^{161}Sm Nilsson-BCS calculations

The Nilsson-BCS calculations for ^{161}Sm are summarized in Table IX, with deformation parameters taken from Möller *et al.* [28]: $\epsilon_2 = 0.275$ and $\epsilon_4 = -0.013$. The calculated $\frac{7}{2}^+[633]$ ground state is in good agreement with the experimental data (Fig. 10) together with the $N = 99$ systematics, and the lowest-energy 3-qp state, with the $K^\pi = \frac{17}{2}^-$, $\nu\frac{7}{2}+[633]\otimes\pi\frac{5}{2}^-[532]\otimes\pi\frac{5}{2}^+[413]$ configuration, can now be associated with the experimental $(\frac{17}{2}^-)$ isomer. The placement of several additional transitions, observed experimentally, remains to be achieved.

D. ^{163}Eu Nilsson-BCS calculations

Nilsson-BCS calculations have been performed to understand the level scheme of ^{163}Eu. The deformation parameters were taken from Möller *et al.* [28]: $\epsilon_2 = 0.275$ and $\epsilon_4 = 0.000$. The results can be seen in Table X.

The lowest energy 1-qp state, with $K^\pi = \frac{5}{2}^+$, is in accord with the experimental systematics for the the $\pi\frac{5}{2}^+[413]$ configuration. The ground states of the isotopes ^{157}Eu [29] and ^{159}Eu [29,30] both have this assignment.

The isomeric state in Fig. 13 is assigned a $(\frac{13}{2}^-)$ spin parity. The lowest 3-qp state in the calculations has the $\pi\frac{5}{2}^+[413]\otimes\pi\frac{5}{2}^-[532]\otimes\pi\frac{3}{2}^+[411]$ configuration with $K^\pi = \frac{13}{2}^-$ and this can reasonably be associated with the experimental state. The experimental and calculated energies differ by only 162 keV.

V. *E*1 REDUCED HINDRANCE FACTORS

As commented on in the introduction, K-forbidden transitions can give rise to long half-lives, which enable a variety of nuclear excited states to be accessed. This feature was

TABLE X. Low-lying qp states in ^{163}Eu, as for ^{162}Sm (see Table VI header).

K^π	Configuration	E_x (MeV)	$E_x^{\rm exp}$ (MeV)
1-qp states			
$\frac{5}{2}^+$	$\pi\frac{5}{2}^+[413]$	0	
$\frac{5}{2}^-$	$\pi\frac{5}{2}^-[532]$	0.073	
$\frac{3}{2}^+$	$\pi\frac{3}{2}^+[411]$	0.134	
$\frac{7}{2}^-$	$\pi\frac{7}{2}^-[523]$	0.726	
3-qp states			
$\frac{13}{2}^-$	$\pi\frac{5}{2}^+[413]\otimes\pi\frac{5}{2}^-[532]\otimes\pi\frac{3}{2}^+[411]$	0.802	0.964(1)
$\frac{13}{2}^-$	$\nu\frac{7}{2}^+[633]\otimes\nu\frac{1}{2}^-[521]\otimes\pi\frac{5}{2}^+[413]$	1.048	
$\frac{13}{2}^+$	$\nu\frac{7}{2}^+[633]\otimes\nu\frac{1}{2}^-[521]\otimes\pi\frac{5}{2}^-[532]$	1.120	
$\frac{11}{2}^-$	$\nu\frac{7}{2}^+[633]\otimes\nu\frac{1}{2}^-[521]\otimes\pi\frac{3}{2}^+[411]$	1.182	
$\frac{17}{2}^+$	$\pi\frac{5}{2}^+[413]\otimes\pi\frac{5}{2}^-[532]\otimes\pi\frac{7}{2}^-[523]$	1.555	
$\frac{17}{2}^+$	$\nu\frac{7}{2}^+[633]\otimes\nu\frac{5}{2}^-[512]\otimes\pi\frac{5}{2}^-[532]$	1.770*	
$\frac{17}{2}^-$	$\nu\frac{7}{2}^+[633]\otimes\nu\frac{5}{2}^-[512]\otimes\pi\frac{5}{2}^+[413]$	1.797*	

evident in the level schemes presented. In this section, a quantitative comparison of the K-forbidden transition rates is made with other similar transitions in the same mass region. To do this, the reduced hindrance [4] is first evaluated as $f_\nu = (T^\gamma_{1/2}/T^W_{1/2})^{1/\nu}$, where $T^\gamma_{1/2}$ is the partial γ-ray half-life, $T^W_{1/2}$ is the corresponding Weisskopf single-particle estimate, and the degree of forbiddenness, $\nu = \Delta K - \lambda$, as defined in Sec. I. In this way, the effects of the transition energy, multipole character, and degree of forbiddenness are approximately accounted for, so that remaining f_ν variations should have a different physical explanation, e.g., from K mixing. For $E1$ transitions it was also shown to be appropriate to multiply their Weisskopf half-lives by 10^4 before evaluation of f_ν, to take account of the generally more-hindered nature of $E1$ transitions [31].

The isomer decays observed in the present work have all been interpreted as K-forbidden $E1$ transitions. In Fig. 18 the systematic behavior of the $Z = 62$ and $N = 100$ $E1$ reduced hindrances is shown, using the present values and those from the literature [3,5,7,8,10,11,32]. The inclusion of the 10^4 factor makes the $\Delta K = 5$ ($Z = 62$) values closer to those for $\Delta K = 4$ ($N = 100$). The data are given in Table XI.

The values for $\Delta K = 5$ are somewhat smaller than those for $\Delta K = 4$, at least for $A \leqslant 170$, but a physical mechanism that causes this was not yet identified. The f_ν values for the $N = 100$, $\Delta K = 4$ transitions in ^{162}Sm, ^{163}Eu, and ^{164}Gd (as reported in the current work) are seen to be almost constant and similar to the other cases of the same type for $A \leqslant 170$. This contrasts with the sudden drop in f_ν for $A > 170$, with relatively small and decreasing f_ν values for ^{172}Hf and ^{174}W. This can be qualitatively understood as arising from a combination of octupole and Coriolis mixing [33], largely from the $\frac{7}{2}^+[633]$, $i_{13/2}$ neutron in the 2-qp configuration. Such mixing increases with decreasing deformation, hence with increasing mass in the present instance. It would be useful to model this effect, although that goes beyond the current work.

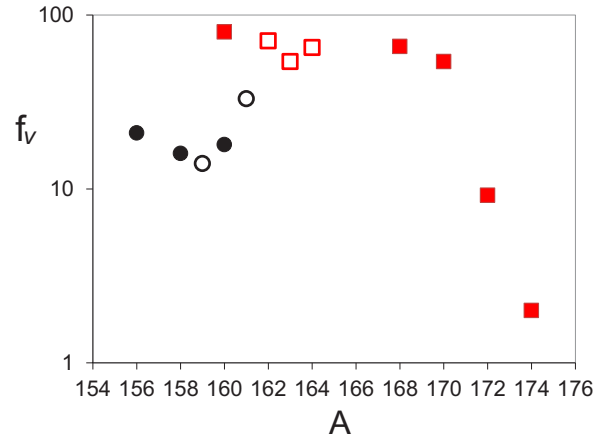

FIG. 18. $E1$ reduced hindrance factors shown as a function of mass number, with the Weisskopf half-lives multiplied by 10^4 (see text). The squares are for $\Delta K = 4$ ($N = 100$) transitions, and the circles are for $\Delta K = 5$ ($Z = 62$). The open symbols correspond to values from the present work.

VI. CONCLUSIONS

Projectile-fission reactions have enabled high-K isomers to be observed in ^{159}Sm, ^{161}Sm, ^{162}Sm, ^{163}Eu, and ^{164}Gd, providing new information about their excited-state structures. After careful consideration of the level schemes and qp configurations, with the use of multi-qp Nilsson-BCS calculations, all the isomeric transitions are interpreted as having K-forbidden $E1$ character. The reduced hindrances are found to be in agreement with the systematic behavior found in the mass region.

TABLE XI. Reduced hindrance values for $E1$ decays from 2- and 3-qp states in $N = 100$ isotones with $\nu = 3$, and $Z = 62$ isotopes with $\nu = 4$, using $T^W_{1/2} \times 10^4$.

Nuclide	K^π	E (keV)	E_γ (keV)	$T_{1/2}$	B_γ (%)	ν	f_ν	Ref.
^{160}Nd	4^-	1108	893	1.6 μs	100	3	80	[8]
^{162}Sm	4^-	1011	775	1.7 μs	100	3	71	This work
^{163}Eu	$13/2^-$	964	675	990 ns	86	3	54	This work
^{164}Gd	4^-	1096	855	530 ns	55	3	65	This work
^{168}Er	4^-	1094	830	109 ns	10	3	66	[3]
^{170}Yb	4^-	1258	981	370 ns	100	3	54	[3]
^{172}Hf	4^-	1418	1109	$\approx$1 ns	80	3	9.2	[3]
^{174}W	4^-	1365	1008	$\approx$17 ps	100	3	2.0	[32]
^{156}Sm	5^-	1398	1148	186 ns	65	4	21	[3,5]
^{158}Sm	5^-	1280	1040	83 ns	64	4	16	[3,5]
^{159}Sm	$15/2^+$	1276	870	115 ns	100	4	14	[11]; this work
^{160}Sm	5^-	1361	1128	120 ns	80	4	18	[5,7]
^{161}Sm	$17/2^-$	1338	883	2.6 μs	$\approx$70	4	33	This work

ACKNOWLEDGMENTS

This work was carried out at the RIBF operated by RIKEN Nishina Center, RIKEN, and CNS, University of Tokyo. All UK authors are supported by STFC. P.H.R. is partially supported by the UK National Measurement Office (NMO). P.-A.S. was financed by JSPS Grant No. 23·01752 and the RIKEN Foreign Postdoctoral Researcher Program. J.T. was financed by Spanish Ministerio de Ciencia e Innovación under Contracts No. FPA2009-13377-C02 and No. FPA2011-29854-C04. Zs.V. and I.K. were supported by OTKA Contract No. K100835. We acknowledge the EUROBALL Owners Committee for the loan of germanium detectors and the PreSpec Collaboration for the readout electronics of the cluster detectors. This work was also supported by JSPS KAKENHI Grant No. 25247045.

[1] R. Surman, J. Engel, J. R. Bennett, and B. S. Meyer, Phys. Rev. Lett. **79**, 1809 (1997).

[2] P. Walker and G. Dracoulis, Nature (London) **399**, 35 (1999).

[3] F. G. Kondev, G. D. Dracoulis, and T. Kibédi, At. Data Nucl. Data Tables **103**, 50 (2015).

[4] G. D. Dracoulis, P. M. Walker, and F. G. Kondev, Rep. Prog. Phys. **79**, 46 (2016).

[5] G. S. Simpson, W. Urban, J. Genevey, R. Orlandi, J. A. Pinston, A. Scherillo, A. G. Smith, J. F. Smith, I. Ahmad, and J. P. Greene, Phys. Rev. C **80**, 024304 (2009).

[6] Z. Patel, P.-A. Söderström, Z. Podolyák, P. H. Regan, P. M. Walker, H. Watanabe, E. Ideguchi, G. S. Simpson, H. L. Liu, S. Nishimura *et al.*, Phys. Rev. Lett. **113**, 262502 (2014).

[7] Z. Patel, Z. Podolyák, P. M. Walker, P. H. Regan, P.-A. Söderström, H. Watanabe, E. Ideguchi, G. S. Simpson, S. Nishimura, F. Browne *et al.*, Phys. Lett. B **753**, 182 (2016).

[8] E. Ideguchi, G. S. Simpson, R. Yokoyama, M. Tanaka, S. Nishimura, P. Doornenbal, G. Lorusso, P.-A. Soderstrom, T. Sumikama, J. Wu *et al.*, Phys. Rev. C **94**, 064322 (2016).

[9] P.-A. Söderström, P. M. Walker, J. Wu, H. L. Liu, P. H. Regan, H. Watanabe, P. Doornenbal, Z. Korkulu, P. Lee, J. J. Liu *et al.*, Phys. Lett. B **762**, 404 (2016).

[10] R. Yokoyama, S. Go, D. Kameda, T. Kubo, N. Inabe, N. Fukuda, H. Takeda, H. Suzuki, K. Yoshida, K. Kusaka *et al.*, Phys. Rev. C **95**, 034313 (2017).

[11] W. Urban, J. A. Pinston, G. S. Simpson, A. G. Smith, J. F. Smith, T. Rząca-Urban, and I. Ahmad, Phys. Rev. C **80**, 037301 (2009).

[12] Z. Patel, Z. Podolyák, P. M. Walker, P. H. Regan, P.-A. Söderström, H. Watanabe, E. Ideguchi, G. S. Simpson, S. Nishimura, F. Browne *et al.*, Eur. Phys. J. Conf. **123**, 02002 (2016).

[13] Y. Yano, Nucl. Instr. Meth. B **261**, 1009 (2007).

[14] T. Kubo, D. Kameda, H. Suzuki, N. Fukuda, H. Takeda, Y. Yanagisawa, M. Ohtake, K. Kusaka, K. Yoshida, N. Inabe *et al.*, Prog. Theor. Exp. Phys. **2012**, 03C003 (2012).

[15] S. Nishimura, Prog. Theor. Exp. Phys. **2012**, 03C006 (2012).

[16] S. Nishimura, Nucl. Phys. News Int. **22**(3), 38 (2012).

[17] P.-A. Söderström, S. Nishimura, P. Doornenbal, G. Lorusso, T. Sumikama, H. Watanabe, Z. Xu, H. Baba, F. Browne, S. Go *et al.*, Nucl. Instr. Meth. B **317**, 649 (2013).

[18] T. Kibédi, T. W. Burrows, M. B. Trzhaskovskaya, P. M. Davidson, and C. W. Nestor, Nucl. Instr. Meth. A **589**, 202 (2008).

[19] E. F. Jones, J. H. Hamilton, P. M. Gore, A. V. Ramayya, J. K. Hwang, A. P. deLima, S. J. Zhu, Y. X. Luo, C. J. Beyer, J. Kormicki *et al.*, J. Phys. G: Nucl. Part. Phys. **30**, L43 (2004).

[20] A. Osa, S. Ichikawa, M. Matsuda, T. K. Sato, and S.-C. Jeong, Nucl. Instr. Meth. B **266**, 4394 (2008).

[21] C. Gautherin, M. Houry, W. Korten, Y. Le Coz, R. Lucas, X. H. Phan, Ch. Theisen, Ch. Badimon, G. Barreau, T. P. Doan *et al.*, Eur. Phys. J. A **1**, 391 (1998).

[22] S. Ichikawa, K. Tsukada, I. Nishinaka, Y. Hatsukawa, H. Iimura, K. Hata, Y. Nagame, A. Osa, M. Asai, Y. Kojima *et al.*, Phys. Rev. C **58**, 1329 (1998).

[23] G. Audi, F. G. Kondev, M. Wang, H. J. Huang, and S. Nami, Chinese Phys. C **41**, 030001 (2017).

[24] Z. Patel, Ph.D. thesis, University of Surrey, 2015.

[25] K. Jain, O. Burglin, G. Dracoulis *et al.*, Nucl. Phys. A **591**, 61 (1995).

[26] K. Jain, P. Walker, and N. Rowley, Phys. Lett. B **322**, 27 (1994).

[27] C. J. Gallagher and S. A. Moszkowski, Phys. Rev. **111**, 1282 (1958).

[28] P. Moller, J. R. Nix, W. D. Myers, and W. J. Swiatecki, At. Data Nucl. Data Tables **59**, 185 (1995).

[29] D. G. Burke, G. Lovhoiden, E. R. Flynn, and J. W. Sunier, Nucl. Phys. A **318**, 77 (1979).

[30] H. Mach, A. Piotrowski, R. L. Gill, R. F. Casten, and D. D. Warner, Phys. Rev. Lett. **56**, 1547 (1986).

[31] P. M. Walker, Phys. Scr. **92**, 054001 (2017).

[32] J. Gascon, P. Taras, P. V. Esbroek, H. R. Andrews, D. C. Radford, D. Ward, and A. Christy, Nucl. Phys. A **472**, 558 (1987).

[33] G. D. Dracoulis, P. M. Walker, and A. Johnston, J. Phys. G **4**, 713 (1978).